STUDIA INFORMATICA 2004
Volume 25 Number 3 (59)

Katarzyna STĄPOR, Adam ŚWITOŃSKI
Politechnika Śląska, Instytut Informatyki

AUTOMATIC DETECTION OF EARLY SYMPTOMS OF DIABETIC RETINOPATHY FROM FUNDUS EYE IMAGES USING MATHEMATICAL MORPHOLOGY

Summary. In this paper the new method for automatic segmentation of microaneurysms from fundus eye images is proposed. It relies on methods from mathematical grayscale morphology. The new *HitAndMiss* transformation has been defined for the detection of markers of watershed transformation.

Keywords: mathematical morphology, HitAndMiss transform, micro-aneurysms, diabetic retinopathy.

AUTOMATYCZNA DETEKCJA WCZESNYCH SYMPTOMÓW RETINOPATII CUKRZYCOWEJ NA CYFROWYCH OBRAZACH DNA OKA ZA POMOCĄ METOD MORFOLOGII MATEMATYCZNEJ

Streszczenie. W artykule przedstawiono nową metodę automatycznej segmentacji mikroaneuryzmatów na cyfrowych obrazach dna oka. Zaproponowana metoda wykorzystuje narzędzia wieloodcieniowej morfologii matematycznej. Zdefiniowano nowe przekształcenie trafi-nie-trafi dla detekcji markerów transformaty wododziałowej.

Słowa kluczowe: morfologia matematyczna, przekształcenie trafi-nie-trafi, mikroaneuryzmaty, retinopatia cukrzycowa.

1. Introduction

Background *diabetic retinopathy* is a severe and widely spread eye disease. It is the commonest cause of legal blindness in the working-age population of developed countries. As its initial stage, the disease sits in the background, with no symptoms. As a result, the patient is oblivious of its presence. At this point, there is not an immediate threat of vision

impairment, but it is the beginning of serious damage to the retina and it is considered to be the first stage of blood vessel deterioration.

The characteristic features of background retinopathy are microaneurysms, haemorrhages and exudates [3]. *Microaneurysms* are discrete, localized saccular distension of the weakened capillary walls, and are present as small, circular red 'dots ' on the retina. *Haemorrhages*, or impairments of the blood-retina barrier, appear either as a red 'dot' or appear 'flame-shaped'. In the latter case, they have a characteristically 'feather-shaped' edge. *Exudates* are caused by proteins and lipids leaking from the blood into the retina via damaged blood vessels. These appear on the ophthalmoscope as hard/harsh white or yellow areas, sometimes in a ring-like structure around leaking capillaries.

Diabetic retinopathy can be treated by laser surgery in which a strong light beam is aimed on to the retina to shrink the abnormal vessels. Laser surgery has been proved to reduce the risk of severe vision loss from background diabetic retinopathy by 90%.

The most dangerous threats to vision in diabetes give little or no warning. Only by direct examination with an ophthalmoscope can these early changes be seen, and hence treatment could start before sight becomes seriously threatened. Therefore, regular retinal examinations of the risk groups are highly recommended. The costs of these examinations and the shortage of specialists, especially in rural areas, are the drawbacks of this procedure. Furthermore, in order to monitor the disease, comparison between the images taken at different examinations is necessary. Up to now, the number of lesions (microaneurysms, exudates) is compared, but it would lead to a more sophisticated diagnosis, if one could compare the evolution of each single lesion. Because this task can hardly be fulfilled manually, a computer assisted approach is required – consisting of detecting lesions in retinal images.

For the above reasons, we think that relying on a robust and fast algorithms for detecting lesions of diabetic retinopathy is crucial point of any computer assistance for the diagnosis of this disease.

This article presents the new method for automatic detection of the most important early symptoms of diabetic retinopathy - the **microaneurysms** (**MAs**) from ordinary, color **fundus eye images** (**fei**).

In automatic retinal analysis, there are two main classes of images in use: "ordinary" color or gray level images, and angiograms. The last class results from photographing the retina after the patient has been injected with a contrast fluid. This makes it easier to detect small details due to the increased image contrast.

The detection of MAs in fluorescein angiograms has been the subject of many publications [1,4,6]. In a case of detecting MAs in color images – MAs appear much less contrasted than in angiograms. It seems that only few researchers have concentrated on MAs

detection from ordinary fundus images [9], and the results presented there are not very impressive (84%).

As the angiographic process is both costly and time-consuming and because the results obtained by the existing algorithms for MAs detection are not very satisfactory we, therefore, decided to devise a totally new method for MAs detection from ordinary, color fei. The proposed new method is composed of the following stages: 1) preprocessing, 2) finding markers, 3) watershed transformation, 4) classification. In this method, the new *HitAndMiss* transformation for grayscale morphology has been defined which can be considered as a counterpart of the existing *HitAndMiss* transformation in binary morphology. As far as we know, no gray-level counterpart of binary *HitAndMiss* transformation has been defined yet.

2. Basic gray-level morphological operators

In this section we briefly define the basic morphological operators used in this paper (for a comprehensive presentation see [5]). Let D_f and D_B be subsets of Z^2 and $T=\{t_{min}, \ldots, t_{max}\}$ be an ordered set of gray levels. A *gray-level image f* can be defined as a function:

$$f : D_f \subset Z^2 \to T \tag{1}$$

Furthermore, we define another image known as a *structuring element B*:

$$B : D_B \subset Z^2 \to T \tag{2}$$

We will restrict to flat, symmetric structuring elements B [5] and assume that point $(0,0) \in D_B$. We can now write the four basic morphological operators: *erosion*, *dilation*, *opening* and *closing* as:

$$E^B(f)(x,y) = \inf_{(j,k)\in D_B}\{f(x-j,y-k)\} \qquad D^B(f)(x,y) = \sup_{(j,k)\in D_B}\{f(x-j,y-k)\} \tag{3}$$

$$O^B(f)(x,y) = D^B(E^B(f)(x,y)) \qquad C^B(f)(x,y) = E^B(D^B(f)(x,y)) \tag{4}$$

Symmetric, *morphological gradient* of an image f can be defined as:

$$grad(f)(x,y) = D^B(f)(x,y) - E^B(f)(x,y) \tag{5}$$

To define watershed transformation (*WT*) we first give some needed definitions. A *section* Z_i of an image f at a level i is defined as:

$$Z_i(f) = \{x \in Z^2 : f(x) \le i\} \tag{6}$$

The *X-reconstructed set* by the marker set $Y \subset X$ is defined as:

$$R_X(Y) = \left\{x \in X : \exists_{y\in Y}\, d_X(x;y) \neq \infty\right\} \tag{7}$$

where $d_X(x,y)$ is the *geodesic distance* (the length of shortest path included in X and linking x and y). Suppose Y is composed of n connected components Y_i ( ).

The *geodesic zone of influence* $Z_X(Y_i)$ of Y_i is defined as:

(8)

The boundaries between the various zones of influence give the *geodesic skeleton* by zones of influence of Y in X:

(9)

Imagine that we pierce each minimum of the topographic surface S of a function f, and that we plunge this surface into a lake with a constant speed. During the flooding, two or more floods coming from different minima may merge. We want to avoid this event and we built a dam on the points on the surface S where the floods would merge. At the end of the process, only the dams emerge. These dams define the *watershed lines* of the function *f*. They separate the various catchment basins, each one containing one and only one minimum of a function *f*.

Consider now a section $Z_i(f)$ of f at level i and suppose that the flood has reached this height. Denote by $W_i(f)$ the the set of points already flooded by a water. Then:

(10)

(11)

This iterative algorithm is initiated with . At the end of the process, the set of watershed lines (i.e. dams) is equal to:

(12)

Normally, the WT is performed on a gradient image and is based on a set of markers M to avoid over-segmentation [1]. Internal markers m_{int} are associated with objects of interest and are the only allowed minima. External markers m_{ext} are associated with the background. Such modified *WT* can be written as follows:

$$W_{i+1}(f) = \left\lfloor IZ_{Z_{i+1}(g)\cup M}(W_i(f)) \right\rfloor \qquad W_{-1}(f) = M = m_{\text{int}} \cup m_{ext} \tag{13}$$

3. The proposed segmentation method for microaneurysms

The proposed segmentation method is composed of the four main steps: 1) preprocessing, 2) finding markers, 3) watershed transformation, 4) classification, which will be described in

the following sections. The proposed method can be integrated in a tool for diagnosis of diabetic retinopathy.

3.1. Properties of microaneurysms

Microaneurysms, the most important early symptoms of diabetic retinopathy, are tiny dilations of the capillaries. They appear as small reddish isolated patterns of circular shape, close to the vascular net in color fundus images of the human retina [3] (see Fig. 1a). Their diameter lies normally between 10 and 100 μm (less than half a typical vessel's width), but it is always smaller than 125 μm. As they come from capillaries, and as capillaries are not visible in color fundus images, they appear as isolated patterns, i.e. disconnected from the vascular tree. One has found that an increase in the number of MAs over time is strongly correlated with the early development of retinopathy. The conventional way of detecting MAs consists in pointing them manually on an image of the retina. This is of course very much time consuming.

3.2. Preprocessing

Although MAs appear as reddish spots, it turns out that they are more distinguishable from the background in the green band image. Thus, we work on the green channel f_G of the color image.

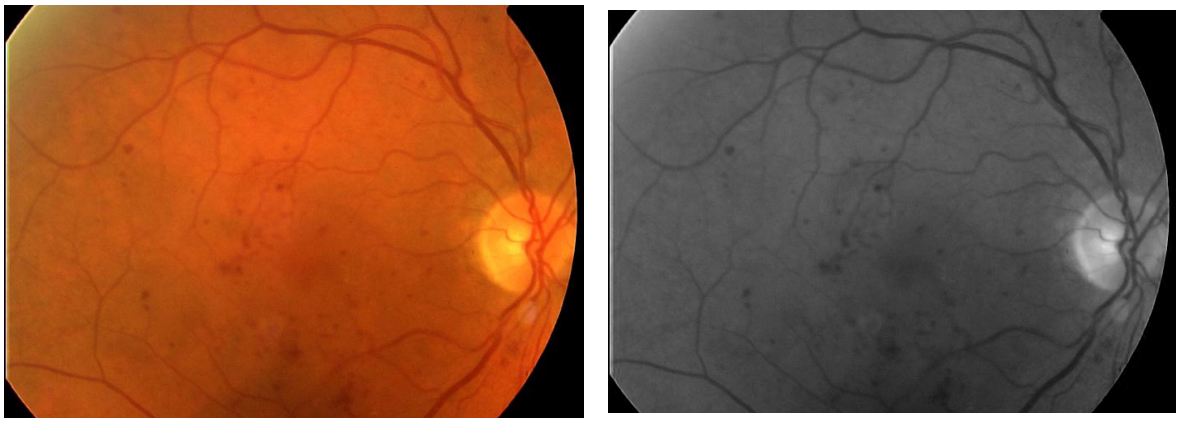

a) b)

Fig. 1. Microaneurysms on fundus eye image: a) RGB format, b) the G channel of the input image shown in Fig.1a)

Rys. 1. Mikroaneuryzmaty na cyfrowym obrazie dna oka: a) format RGB, b) kanał G obrazu wejściowego z rys. 1a)

One of the main differences between angiographies and the green channel of color images is the lower contrast of the latter ones. Due to uneven intensity of illumination, the

background of a retinal image typically has a slowly varying nonuniform intensity. Moreover, these images are also often very noisy.

Nonuniform intensity makes some operations of image thresholding more troublesome. The farther from the image center, the darker the background typically is. We thus apply a shade-correction operator in order to remove slow background variations. The whole background normalization can be described by the following transformation of the input image f_G:

(14)

where *k* is a positive constant and

(15)

is the result of alternating sequential filtering [5] of f_G (*n=31* in our case). This is the approximation of the slow variations of the background of image f_G.

Then we smooth the resulted image by morphological filtering consisted of gray-level morphological opening followed by a closing operation with a flat structuring element B being a 3x3 square.

$$f_G^2 = C^B(O^B(f_G^1)) \tag{16}$$

3.3. Finding markers

Finding the contours of MAs is based on the morphological watershed transformation [5] of the image f_G^2 with the properly found set of internal and external markers.

The procedure for marker detection is based on the new, proposed $HitMiss_G$ transformation. For the detection of the positions of near circular spots (i.e. MAs) within a certain range of sizes we defined the new transformation:

$$HitMiss_G(f, A, B)(x, y) = E(f, A)(x, y) - D(f, B)(x, y) \tag{17}$$

where: f - input image,
A, B - structural elements,

which we call $HitMiss_G$ because of its similarity (in results only) to popular *HitAndMiss* transformation [5] in binary morphology. The input image *f* is eroded first using a structuring element *A*, then dilation with a structuring element *B* is performed on a copy of image *f*, and the difference of the results of these two operations is taken as the final result. As far as we know, no gray-level counterpart of binary *HitAndMiss* transformation has been defined yet.

We thus use the defined above $HitAndMiss_G$ transformation for the detection of the position of MAs in the preprocessed image f_G^2:

(18)

The example of a pair of the structuring elements *A* and *B* that can be used to extract MAs is shown in Fig.2. In our case, two pairs of such structuring elements have been used: one for small MAs (diameter *2* and *7*), and one for large (diameter *4* and *11*).

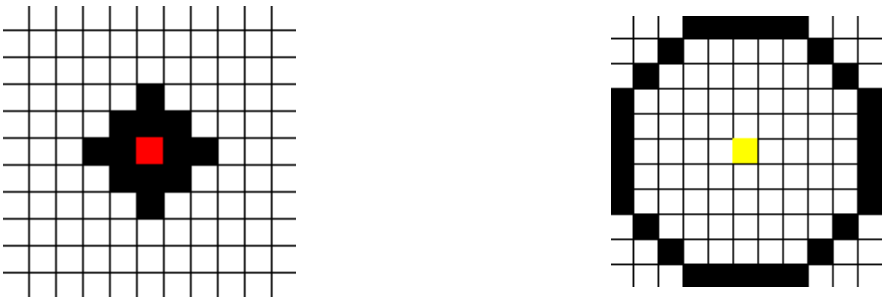

a) b)

Fig. 2. Structuring elements used in HitAndMiss_G transformation: a) element A, b) element B

Rys. 2. Elementy strukturalne używane w przekształceniu HitAndMiss_G: a) element A, b) element B

On the resulted image after $HitMiss_G$ operation we performed global binarization:

(19)

with a threshold *T1* experimentally set (*3* in our case). The resulted "points" indicating positions of MAs are taken as internal markers m_{int} in watershed transformation. The above algorithm will produce some false spots (positions of them) that are really parts of vessels. They will be eliminated in further classification step.

As external markers m_{ext} we use circles, each of them with a center at one of the detected "points" from m_{int} set and a radius bigger than the diameter of the greatest MAs (Fig.3.).

3.4. Watershed transformation

In order to detect exact contours of the MAs, we apply the classical watershed transformation [5]:

$$f_G^5 = WT^{m_{\text{int}} \cup m_{ext}}(f_G^4) \tag{20}$$

to the morphological gradient of the preprocessed image f_G^2:

$$f_G^4 = grad(f_G^2) = D^B(f_G^2) - E^B(f_G^2) \tag{21}$$

1. with internal m_{int} and external m_{ext} markers imposed to avoid over-segmentation of the image. We use a flat structuring element B being a square of size 3x3. The watershed transformation assigns to each local minimum of one catchment basin (one connected region), in a way that all belong to a basin except a one pixel strong line that delimits the basins (the watershed line). The detected exact contours of the MAs after classification step (e.g. elimination of false positives) are shown in Fig 4 superimposed on the input image.

Fig. 3. The set of internal (white points) and external markers (black circles) superimposed on the input image
Rys. 3. Zbiór wewnętrznych (białe punkty) oraz zewnętrznych markerów (czarne okręgi) nałożony na obraz wejściowy

3.5. Classification

Many shape characteristics have been proposed in the literature [4,6] in order to distinguish between true MAs and false positives. (e.g. the perimeter, circularity) in angiographies. However, we found that most of these characteristics are meaningful only for high resolution images. Over and above that, they must rely on a robust segmentation algorithm for the candidate regions, that can easily be conceived for angiographies, but not for color images because of low contrast. The elimination of false positives is based on methods proposed in [9]. We found the best results for the following criteria:

2. **The position**. The MAs cannot be situated neither on the vascular tree nor on the optic disc. Hence, we detect the vessels [7] and the optic disc [8], and we remove all candidates on these features.
3. **The area.** Often we have a relatively high amount of high amplitude pixel noise. Hence, we simply remove all candidates that have an area smaller than a certain value (we assumed in our images, that the area of the candidates must be larger than 3 pixels).
4. **The local contrast criterion**. We calculate the difference between the mean value within the candidate region and the mean value on the outside of it. If this criterion is smaller than a parameter k (in our case good results were found for $k=8$), we reject the candidate.

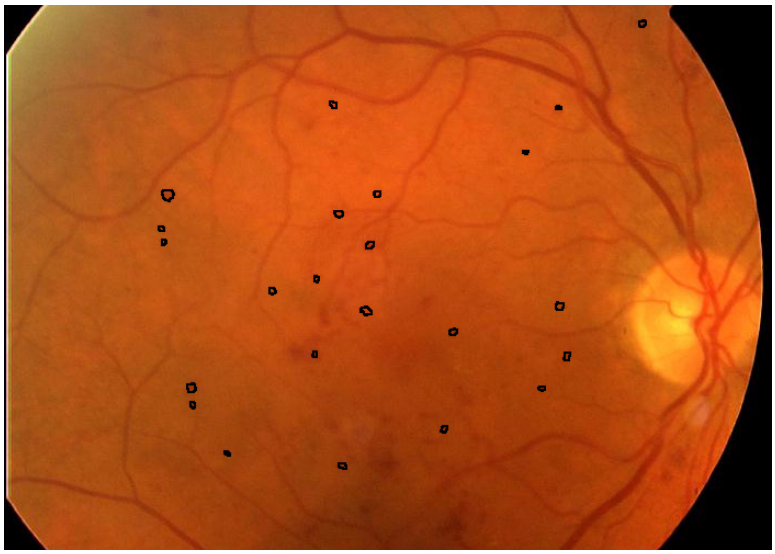

Fig. 4. The contours of the detected MAs superimposed on the input image
Rys. 4. Kontury wysegmentowanych mikroaneuryzmatów nałożone na obraz wejściowy

4. Results and conclusions

At the moment, we cannot present a clinical validation of the algorithm, but just a preliminary test. The algorithm has been tested on 50 images taken with SONY color video 3CCD camera on a Topcon TRC 50 IA retinograph. These images have not been used for the development of the algorithm. The images contained 112 MAs (marked by a human grader). Of these MAs, 89.4% were detected by the proposed algorithm (sensitivity). We also detected false positives (FP), so that the predictive value, i.e. the ratio:

$$TP/(TP+FP) \tag{22}$$

which is the probability that a detected MA is really MA, with *TP*, the correctly classified MAs (true positives *TP*) was 78.8%.

Most of these false positives were situated on bigger hemorrhages or on very small low contrasted vessels that have not been detected by the vessel detection algorithm.

MAs can also easily be confounded with intraretinal microvascular abnormalities and small hemorrhages, but it might be very hard for an algorithm to distinguish between these lesions, because even for human graders, the distinction is sometimes hard to make.

Compared to the results found in [6,9], we obtain a better sensitivity (the Authors obtained *82%* and *84%*, respectively). Figure 4 shows the results obtained by the presented algorithm on the exampled fei shown in Figure 1a).

The performance is satisfying, but the clinical validation is still in progress. This algorithm shall be a part of a bigger software tool for supporting diabetic retinopathy diagnosis and monitoring which is under development.

The algorithm could be improved by using algorithm for detection hemorrhages. A second way to improve the performance of the algorithm is the optimization of the classification step; where more properties and classification method with learning phase can be used.

REFERENCES

1. Frame A. et al: A comparison of computer-based classification methods applied to the detection of microaneurysms in ophthalmic fluorescein angiograms. Computers in Biology and Medicine, v. 28, 1998, 225-238.
5. Gonzalez R.C, Woods R.E: Digital Image Processing. Prentice-Hall, 2002.
6. Kanski J. et al.: Clinical ophthalmology. Butterworth-Heinemann, 1996.
7. Mendonca A. M. et al: Automatic segmentation of microaneurysms in retinal angiograms of diabetic patients, Proc. ICIAP, 1999, 728-733.
8. Soille P.: Morphological image analysis: principles and applications. Springer-Verlag, Berlin 1999.
9. Spencer T. et al: An image processing strategy for the segmentation and quantification of microaneurysms in fluorescein angiograms of the ocular fundus. Computers and Biomedical Research, v. 29, 1996, 284-302.
10. Stąpor K., Świtoński A.: Blood vessel segmentation from color fundus eye images using methods of mathematical morphology. Studia Informatica, submitted for publication.

11. Stąpor K. et al.: Automatic analysis of fundus eye images for detection of glaucomatous changes. Archives of Theoretical and Applied Computer Science, V.15, Nr 2, 2003, 169-184.
12. Walter T., Klein C.: Automatic detection of microaneurysms in color fundus images of the human retina by means of the bounding box closing. In: A. Colosimo et. al. (Eds): Lecture Notes in Computer Science, v. 2526, 2002, 210-220.

Recenzent: Dr inż. Henryk Palus

Wpłynęło do Redakcji 31 marca 2004 r.

Omówienie

W artykule przedstawiono nowa metodę automatycznej segmentacji mikroaneuryzmatów na kolorowych, cyfrowych obrazach dna oka pozyskanych z funduskamery. Zaproponowana metoda składa się z następujących kroków: 1) przetwarzanie wstępne, 2) detekcja markerów dla transformaty wododziałowej, 3) transformata wododziałowa, 4) klasyfikacja. W celu automatycznej detekcji markerów wewnętrznych dla transformaty wododziałowej zdefiniowano nowe przekształcenie trafi-nie-trafi w morfologii wieloodcieniowej, które może stanowić odpowiednik istniejącego przekształcenia trafi-nie-trafi w morfologii binarnej. Uzyskana średnia sprawność metody wynosi 89,4% i jest wyższa od wyników otrzymanych w metodach poprzedników (84%). Opracowany algorytm detekcji wczesnych stadiów retinopatii cukrzycowej może stanowić jeden z modułów systemu komputerowego wspomagającego diagnozowanie oraz monitorowanie tej choroby.

Adresses

Katarzyna STĄPOR: Politechnika Śląska, Instytut Informatyki, ul. Akademicka 16, 44-100 Gliwice, Polska, delta@ivp.iinf.polsl.gliwice.pl .
Adam ŚWITOŃSKI, Politechnika Śląska, Instytut Informatyki, ul. Akademicka 16, 44-100 Gliwice, Polska.